Available online at www.sciencedirect.com
ScienceDirect
Trans. Nonferrous Met. Soc. China 28(2018) 1705−1713
Transactions of Nonferrous Metals Society of China
www.tnmsc.cn

Improvement in dry sliding wear resistance of Al−17Si−5Cu alloy after an enhanced heat treatment process

Biplab HAZRA, Pankaj BARANWAL, Supriya BERA, Bijay Kumar SHOW

Department of Metallurgical and Materials Engineering,
National Institute of Technology Durgapur, West Bengal, 713209, India

Received 9 November 2017; accepted 3 February 2018

Abstract: To improve the wear resistance of cast Al−17Si−5Cu alloy (AR alloy), isothermal heat treatment is employed to modify the morphology of Si particles (particularly eutectic Si particles). Furthermore, wear behaviour of heat-treated alloy (HT alloy) along with AR alloy is studied using a pin-on-disc tribometer. Worn surfaces are then characterised using scanning electron microscope. The result reveals considerable microstructural modifications after the heat treatment. Accordingly, higher hardness value in HT alloy is obtained compared with AR alloy. The overall wear rate for HT alloy is found to be significantly lower compared with AR alloy at all the applied loads, indicating remarkable improvement in wear resistance. Eutectic Si particles become from acicular/rod-like to spherical/equiaxed morphology (aspect ratio close to 1) on heat treatment, resulting in good bonding with the matrix. Thus, they remain intact during wear and being harder, providing resistance to wear. Moreover, the increased hardness on heat treatment causes further resistance to wear. Therefore, the combined effect of intact harder Si particles on the wearing surface and higher hardness results in superior wear behavior in HT alloy at all loads compared with AR alloy.
Key words: heat treatment; abrasive wear; hypereutectic Al−Si alloys

1 Introduction

Cast Al−Si alloys have widespread applications in various important components for automobile sector due to their excellent combination of properties [1]. Among various Al casting alloys, Al−Si alloys are being used extensively, particularly in the transportation industry [2]. However, in recent years, hypereutectic Al−Si alloy has become an attractive area of research due to its potential to replace cast iron parts in automobile applications [1]. The morphology, size and distribution of primary as well as eutectic silicon crystals in these alloys greatly affect their properties. Both refinement and modification of primary and eutectic silicon and controlling the solidification parameters are reported to enhance the mechanical properties of hypereutectic Al−Si alloy [1].

On the other hand, tribological properties of cast hypereutectic Al−Si alloys need to be investigated for successful application of these alloys as engine block materials. Like mechanical properties, wear behavior is also greatly dependent on size, shape and amount of different microstructural constituents. HU et al [3] reported improved wear resistance in Al−16Si−4Cu−0.5Mg alloy after microstructural modifications. Wear studies on Al−Si alloys with varying Si content and other alloying elements under dry sliding conditions have been studied for many years [4,5]. These studies used various test configurations under various loads and sliding speeds. However, detailed evaluation of wear behavior and the mechanisms of wear are limited.

Among different Al−Si alloys, hypereutectic Al−Si alloys are found to have applications in engine components owing to their good resistance to wear. Al−Si alloys, used as an engine block material in the linerless Chevrolet Vega 2300 engine, was a hypereutectic A390 alloy which was first introduced at the AFS Casting Congress [6]. After successful use in the Vega, A390 alloy was later used in Chevrolet Corvette ZL1, Porsche 928, Mercedes 3.8L V8, and other engines [7]. However, their application has been restricted to luxurious vehicles only due to higher production cost. Improved wear properties in these Al−Si alloys are achieved primarily because of the presence of harder silicon particles in the aluminum matrix. It has been reported [8] that, not only strength but also wear

Corresponding author: Bijay Kumar SHOW; Tel: +91-343-2754739; Fax: +91-343-2547375; E-mail: bijayshow@gmail.com
DOI: 10.1016/S1003-6326(18)64814-9

resistance increases with increase in amount of Si content. However, a refined and uniform microstructure is difficult to obtain using a conversional ingot metallurgical process [9]. Furthermore, increased Si results in poor machinability and castability. Si particles, particularly eutectic Si particles, are present irregularly as long rods with high aspect ratio. Thus, hypereutectic Al−Si alloys are generally treated with various modifiers and grain refiners (like phosphorus) to get refinement/ modification of both primary and eutectic silicon. However, their effect and mechanism of working are still at the initial stages of research. Moreover, application of semi-solid heat treatment to modify Si particles has less been reported. FATHY [10] reported the effect of semi-solid heat treatment on the microstructural evaluation of Al−Si alloys containing 18% Si. In this investigation, effect of semi-solid isothermal heat treatment on the size and shape of primary Si and α(Al) grain has been studied. However, detailed study was not taken up.

Therefore, the goal of the current research is to study tribological behaviour of a Al−17Si−5Cu alloy after microstructural modification using semi-solid heat treatment. Accordingly, semi-solid heat treatment is employed in an as-cast Al−17Si−5Cu alloy (AR alloy) to modify the morphology of Si particles. Detailed tribological study was taken up under dry sliding condition.

2 Experimental

2.1 Material and heat treatment

As-received cast hypereutectic Al−17Si−5Cu alloy (AR alloy) was used for the present work. Standard samples for further characterization were machined from a block of approximately 25 mm in diameter. Samples of 15 mm × 15 mm were prepared for optical metallography and hardness measurement. Cylindrical wear pins (ϕ=6 mm, L=30 mm) were also prepared. One set of samples were subjected to isothermal heat treatment process to modify the as-cast microstructure. Heat treatment (in the semi-solid region) parameters were optimized by varying temperature, soaking time and cooling rate. Thus, the present heat treatment was carried out at temperature of 590 °C (as liquidus and solidus temperatures are 648 and 577 °C, respectively, as per phase diagram of Al−Si alloy). The specimens were heated at 590 °C for 15 min in a muffle furnace followed by warm water (60 °C) quenching. Accordingly, the heat-treated sample was designated as HT alloy.

2.2 Optical and scanning electron microscopy

Specimens for microstructural characterisation were polished initially in various abrasive papers after spreading kerosene and paraffin mixture (mass ratio of 1:1) on these papers. Thereafter, they were polished in cloth with alumina abrasive. To reveal the grains and other features, the polished specimens were etched with Keller's reagent. Detailed microstructural investigations were then carried out in optical microscope (Leica DM 2500 M) equipped with image analysis facility as well as in field emission scanning electron microscope (JEOL, JSM−5800, Japan). α(Al) grain size was calculated by standard linear intercept method [11]. Besides, the average size and aspect ratio of primary as well as eutectic Si particles were measured as per the method described in a published article by the corresponding author of the present study [12] from both optical and scanning electron microscope (SEM) images. Moreover, worn surfaces after dry sliding wear test (to be discussed in section 2.4) were characterized in SEM to ascertain wear mechanisms.

2.3 Hardness test

Hardness values of AR and the HT specimens were obtained in a Vicker's hardness tester (BV 250 (S), BIE, Miraj, India) with 196 N load. Furthermore, micro-hardness tests were conducted on various worn surfaces as well as on virgin surfaces to find the strain hardening effects after wear test using a microhardness tester (MMT-X7B, Hibiki Co., Japan) with 0.49 N load.

2.4 Dry sliding wear test

Wear test under dry sliding condition for various specimens was conducted in a pin-on-disk tribometer (Wear and friction monitor, TR-20LE-PHM 400-CHM-400, DUCOM, India) following standard guidelines [13]. The experimental set-up along with the pin-disk contact (schematic) is presented in Fig. 1. EN 31 steel was used as the counter disk material having hardness of HRC 60 which rotated at a speed of 200 r/min. Three loads of 20, 40 and 60 N, respectively, were used in the present work. Sliding speed of 1.0 m/s was maintained for all the tests and the tests were conducted for 32 min. Both the pin surface and the disk

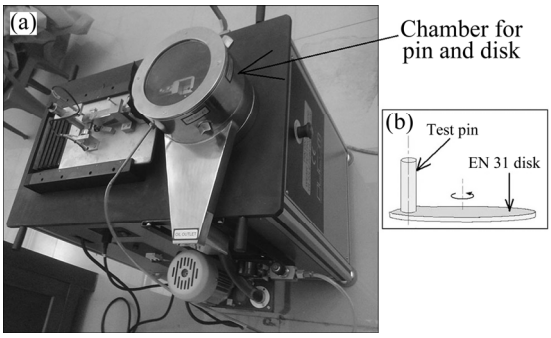

Fig. 1 Wear testing apparatus: (a) Set-up; (b) Schematic of pin-on-disk

were polished in 800 grade abrasive paper prior to each test. Mass loss of the pin was calculated by weighing the pin in a microbalance (CPA225D, Sartorius, Germany) (accuracy of 0.01 mg) before and after the test. Thereafter, wear rate was calculated from the mass loss data. Moreover, cumulative wear data with time were recorded in a computer attached with the instrument. For each condition, two numbers of tests were carried out in order to check the repeatability of test data. The results indicate excellent reproducibility with a standard deviation of less than 5%.

3 Result and discussion

3.1 Microstructure and property characterization

Optical and SEM microstructures of AR alloy (Fig. 2) exhibit the presence of primary Si particles along with α(Al) grains and eutectic phase. The size of the primary Si particles is (17±1.7) μm with an aspect ratio of 1.5±0.26 (Table 1). However, Si particles (with size of (8±1.2) μm) of eutectic phase have long rod/acicular morphology with an aspect ratio of 7±1.3 (Table 1), as opposed to the primary Si particles which are nearly equiaxed/spherical (Fig. 2(b)) in morphology. Eutectic Si particles are found to possess a variety of morphologies and are randomly distributed. The α(Al) grains in as-cast alloy possess variation in size with an average grain size of (26±6) μm.

In HT alloy, semi-solid heat treatment results in considerable improvement in the size as well as aspect ratio for both primary and eutectic Si particles. Figures 3(a) and (b) depict the optical and SEM microstructures of HT alloy, respectively. Optical microstructure of HT alloy (Fig. 3(a)) clearly shows the uniform distribution of particles (both primary and eutectic Si) throughout the microstructure. The eutectic Si particles are found to possess nearly equiaxed/globular morphology with an aspect ratio of 1.3±0.02. The reduction in aspect ratio is due to the minimization in surface energy of liquid phase when the sample is heated in the semi-solid region. This minimization of surface energy leads to the formation of spherical/equiaxed morphology of Si particles. In addition, there is a reduction in eutectic Si particle size in HT alloy as given in Table 1.

Table 1 Mean particle size and aspect ratio of primary and eutectic Si particles in AR and HT alloy

Sample	Si particle	Aspect ratio	Particle size/μm
AR	Primary	1.5±0.26	17±1.7
	Eutectic	7±1.3	8±1.2
HT	Primary	1.4±0.2	15±1.5
	Eutectic	1.3±0.02	7±1.0

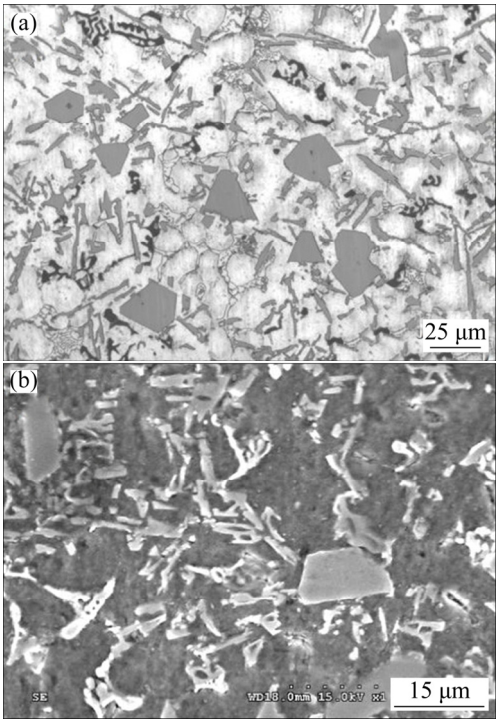

Fig. 2 Microstructural characterization of AR alloy: (a) Overall image; (b) SEM micrograph

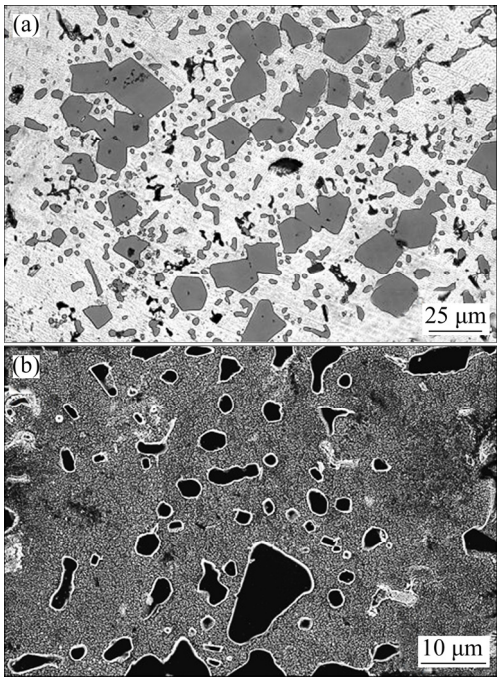

Fig. 3 Microstructural characterization of HT alloy: (a) Overall image; (b) SEM micrograph

Accordingly, improved hardness value (Table 2) is obtained in HT alloy. The increase in hardness is attributed to faster cooling in water after isothermal holding at 590 °C. Thus, matrix retains more solute on faster cooling, resulting in solid solution strengthening in HT alloy. Furthermore, refinement and uniform distribution of eutectic Si particles in HT alloy contribute to higher hardness. Table 1 represents the shape (in terms

of aspect ratio) and size (in terms of average particle diameter) of primary as well as eutectic Si particles for AR and HT alloy. There is a marginal improvement in size and shape of primary Si particles. On the other hand, on heat treatment, there is a considerable improvement in aspect ratio from a value of 7±1.3 in AR alloy to a value of 1.3±0.02 in HT alloy. In addition, there is a reduction in eutectic Si particle size in HT alloy.

Table 2 Bulk hardness values for AR and HT alloy

Sample	Hardness (HVN)
AR	111±4.5
HT	135±9.8

3.2 Wear behaviour

3.2.1 Wear mechanism

3.2.1.1 Wear behaviour of as-received (AR) alloy

The changes in wear loss and coefficient of friction with varying sliding distance at various applied loads for AR alloy are represented in Fig. 4. At 20 N load, wear loss increases linearly with sliding distance (Fig. 4(a)) after a short period of very high loss in wear. This initial high wear loss is mainly due to insufficient strain hardening owing to lower load and less elapsed time. Accordingly, friction coefficient does not vary much with time/sliding distance, as shown in Fig. 4(b). Worn surface images at 20 N load are shown in Fig. 5. Abrasion/scoring marks are clearly visible along with zones of adhesion in low magnification image in Fig. 5(a). Adhesion region containing cracks and delaminated areas are depicted at higher magnification in Fig. 5(b). Continued wear results in strain hardening in the surface and subsurface region. Cracks eventually develop in those regions with progress of wear, which grow and get interconnected, and finally a layer of material is removed in the form of sheet. This is called delamination wear. In addition, materials are also removed from pin by abrasive interaction of the pin with the harder counter disk. This results in abrasion/scoring marks on the worn surface, as shown in Fig. 5(c). The process by which this type of wear occurs is known as microcutting process. Apart from abrasion marks, mild oxidation is also evident from Fig. 5(c) as a few oxide particles are seen on the worn surface. Thus, wear at 20 N load occurs through microcutting abrasion, delamination and mild oxidation. Furthermore, the impressions of removed particle are also clearly seen in Fig. 5(b), indicating poor bonding of particle with the matrix.

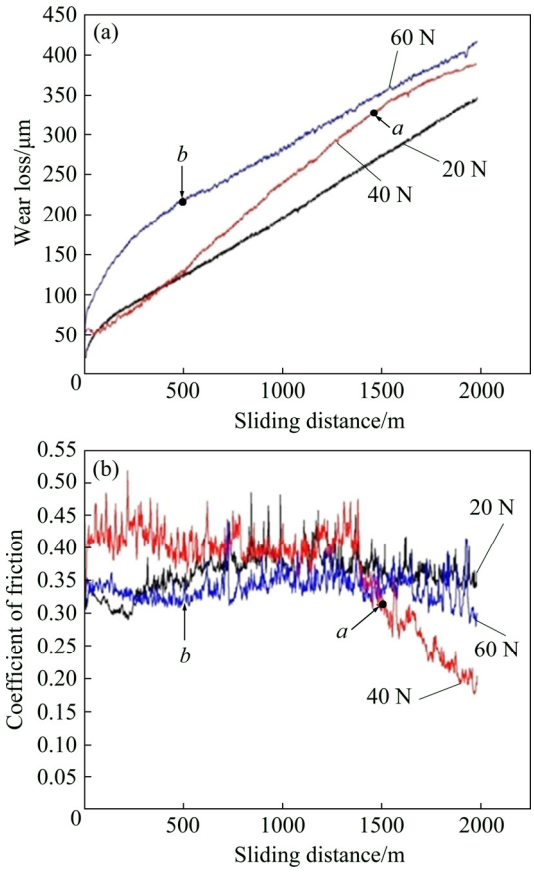

Fig. 4 Changes in wear loss (a) and coefficient of friction (b) as function of sliding distance for AR alloy

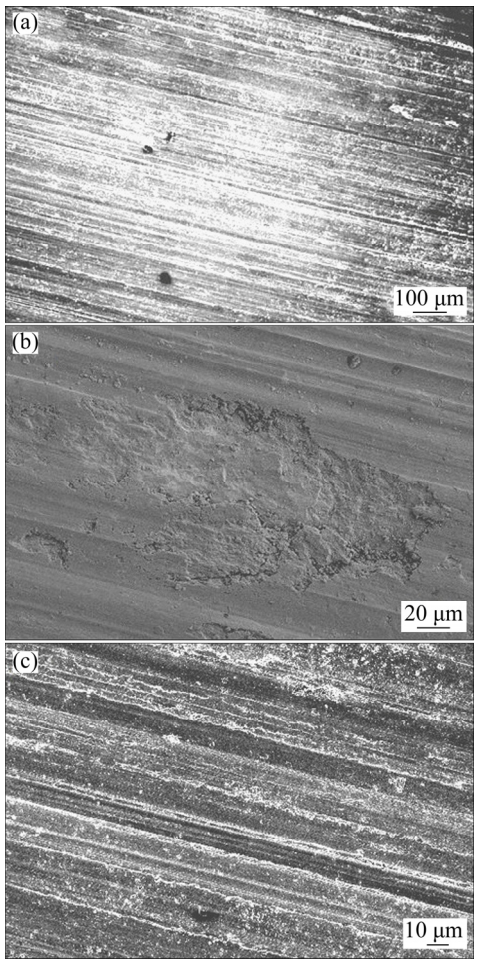

Fig. 5 Worn surface morphologies of AR alloy at 20 N: (a) Overall image; (b) Adhesion region; (c) Abrasion marks and oxides

At 40 N load, wear (cumulative) loss consistently varies with time/sliding distance till point *a* (corresponding to a sliding distance of 1500 m approximately) in Fig. 4(a). Cumulative wear then increases with a decreasing rate with sliding distance beyond point *a* (Fig. 4(a)). The worn surface morphology at 40 N load is shown in Fig. 6. Abrasion marks along with dense adherent layers of oxide are seen in Fig. 6(a). However, abrasion marks are wider (Fig. 6(c)) here, compared to 20 N load (Fig. 5(c)), resulting in larger slope in the linear portion at 40 N load as opposed to 20 N load. Furthermore, prominent adhesive wear zones (Fig. 6(b)) also account for higher total cumulative wear under this load. Like in 20 N load, the impressions of removed particle are also clearly seen in Fig. 6(b), due to poor bonding of particle with the matrix. The formation of adherent oxide layer as shown in Fig. 6(a) is responsible for decrease in rate of cumulative wear ahead of point *a* (Fig. 4(a)). Accordingly, the friction coefficient (Fig. 4(b)) shows less variations with time/sliding distance till point *a* in Fig. 4(b) and then decreases with deceleration of wear loss (between sliding distance of 1500−2000 m), mainly due to formation of oxides.

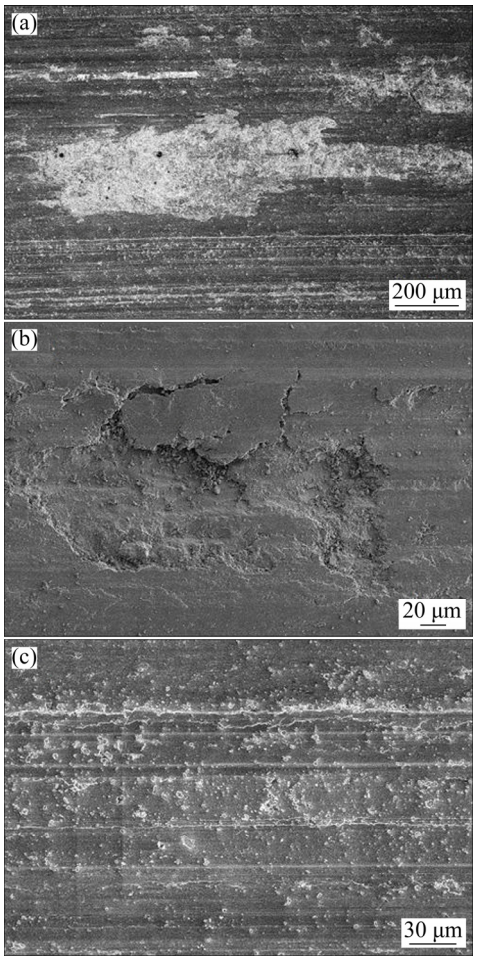

Fig. 6 Worn surface morphologies of AR alloy at 40 N: (a) Overall image; (b) Adhesion region; (c) Abrasion marks and oxides

Wear test results at 60 N load exhibits decreased rate of wear (till point *b* in Fig. 4(a)) initially followed by a linear increment of wear with time/sliding distance. Accordingly, coefficient of friction is found to be less during the initial period followed by steady variation with minor fluctuations (Fig. 4(b)). The worn surface images are presented in Fig. 7. Marks of abrasion/scoring along with traces of thick adherent nodular oxide can be seen from worn surface image shown in Fig. 7(a)). The abrasion marks are deeper (Fig. 7(c)) compared to lower loads, which is attributed to higher initial wear. However, the increase in rate of wear loss is slowed down due to the formation of oxide layers. At higher load (60 N), oxidation occurs and this results in the formation of adherent oxides at the specimen/pin surface due to the increase in pin temperature as a result of frictional heating. Temperature rise at pin surface due to frictional force has also been reported in literatures [14,15]. Oxide layer being adherent, hinders the direct pin to disk contact and thus acts as solid lubricant [16], which results in less wear. It has been reported that the effect of tribo layer (i.e., adherent oxide layer) depends on the strength of the matrix [17]. Tribo layers are more effective in reducing wear rate at room temperature

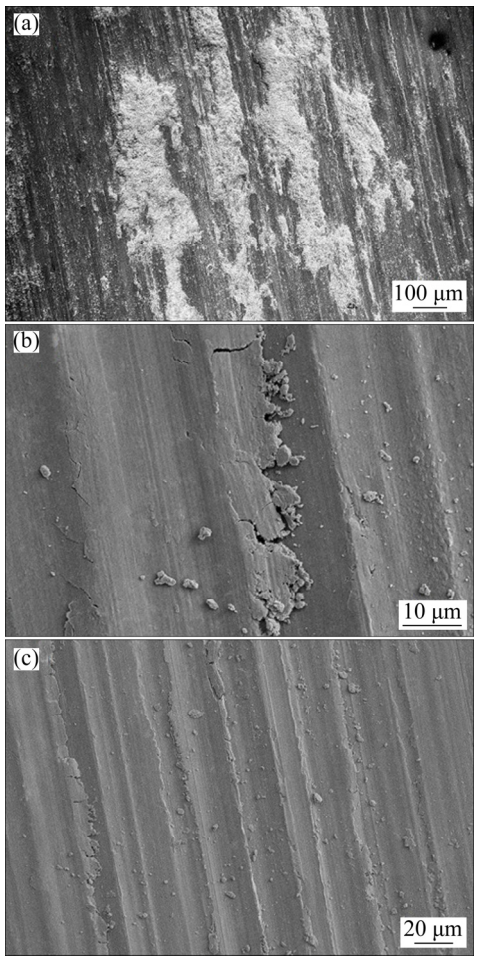

Fig. 7 Worn surface morphologies of AR alloy at 60 N: (a) Overall image; (b) Adhesion region; (c) Abrasion marks

compared to higher temperature where matrix strength is reduced. As the present investigation also deals with room temperature wear, adherent oxide layers are expected to act as solid lubricant and provide resistance to wear loss. Moreover, it is also reported that wear loss in oxidative wear region is less at low sliding speed (≤1 m/s) [18] which is also applicable in the present work. Thus, being adherent, oxides could not be removed easily and their presence can be seen on the worn surface in Fig. 7(a).

3.2.1.2 Wear behaviour of HT alloy

At 20 N load, worn surface image of HT alloy shows mainly abrasion marks (Fig. 8(a)). On the other hand, adhesion region along with the presence of crack is observed in Fig. 8(b). In addition, mild oxidation on the worn surface (Fig. 8(a)) is also evident. Thus, simultaneous abrasive and adhesive wear results in linear variation (after point *a* in Fig. 9(a)) in cumulative wear loss with time/sliding distance. In concurrence, the coefficient of friction also remains steady without much fluctuation with sliding distance (after point *a* in Fig. 9(b)). Though during initial period (up to point *a* in Fig. 9(a)), wear loss is more, the rate of wear loss decreases with time/sliding distance (probably due to strain hardening). Accordingly, coefficient of friction has slightly lower but steady value up to point *a* in Fig. 9(b). It is to be noted that, unlike AR alloy at 20 N load, here Si particles are found to remain intact on the worn surface (Fig. 8(c)), which results in more wear resistance as these harder Si particles provide resistance to abrasive wear. Equiaxed/spherical Si particle morphology provides good bonding with the matrix due to lowering of surface area and thus remains contact during wear.

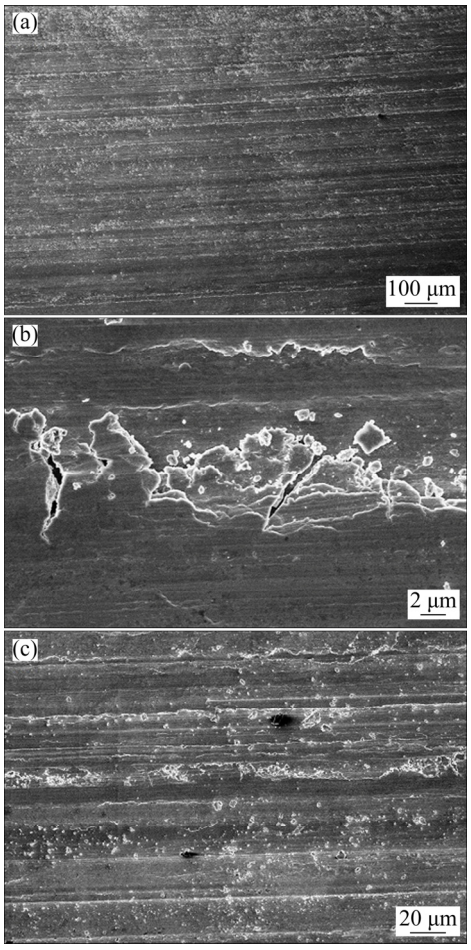

Fig. 8 Worn surface morphologies of HT alloy at 20 N load: (a) Overall image; (b) Adhesion region; (c) Abrasion marks

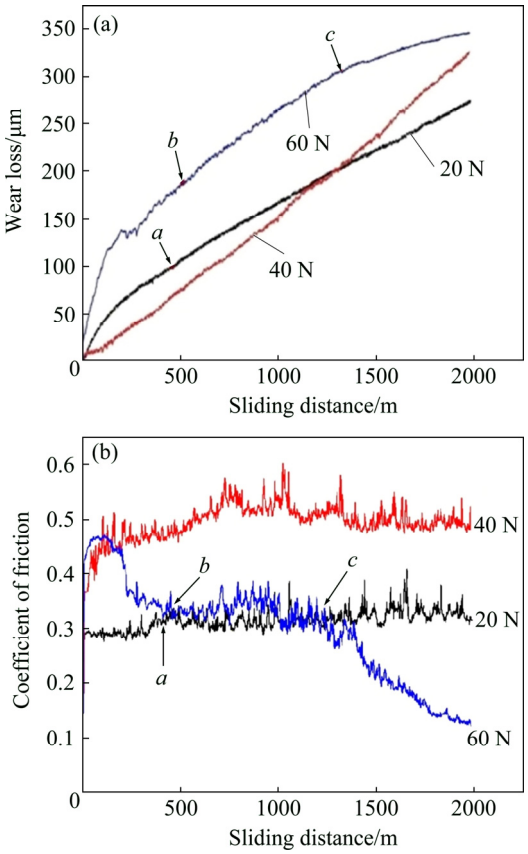

Fig. 9 Changes of wear loss (a) and coefficient of friction (b) as function of sliding distance for HT alloy

At 40 N applied load, the wear behaviour of HT alloy exhibits continuous wear loss with sliding distance (Fig. 9(a)) and coefficient of friction maintains somewhat constant value except some fluctuations (Fig. 9(b)). However, the rate at which wear loss occurs is higher compared with 20 N load. Figure 10 represents worn surface morphology at 40 N load. The abrasion marks are wider and deeper compared with 20 N load, as shown in Fig. 10(c). This accounts for larger slope of the plot in Fig. 9(a) for 40 N load as opposed to 20 N load. Overall worn surface (Fig. 10(a)) exhibits the presence of abrasion marks along with some oxidation. Presence of Si particles along with adhesion and abrasion marks is also prominent on the worn surface (Fig. 10(b)). These Si particles provide resistance to abrasive wear, resulting in better wear resistance compared with AR alloy.

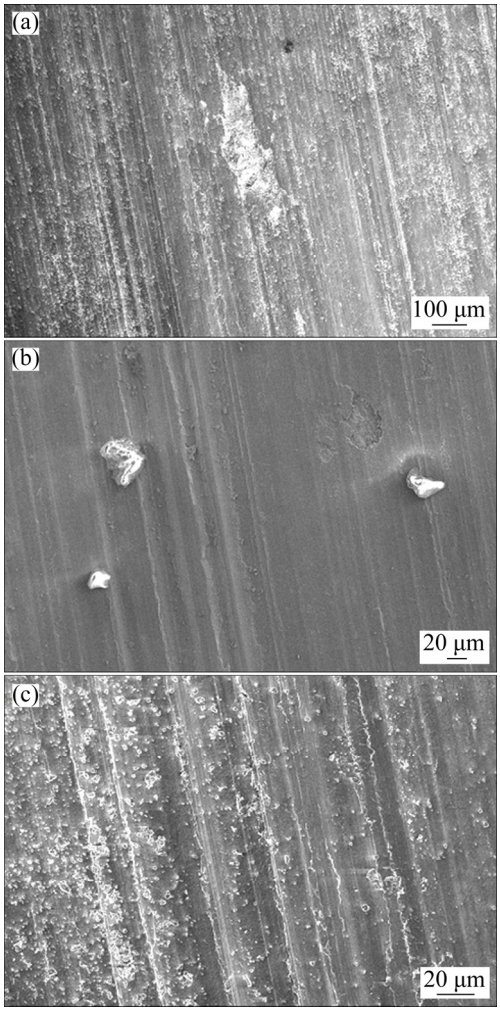

Fig. 10 Worn surface morphologies of HT alloy at 40 N load: (a) Overall image; (b) Adhesion region and presence of intact Si particle; (c) Abrasion marks

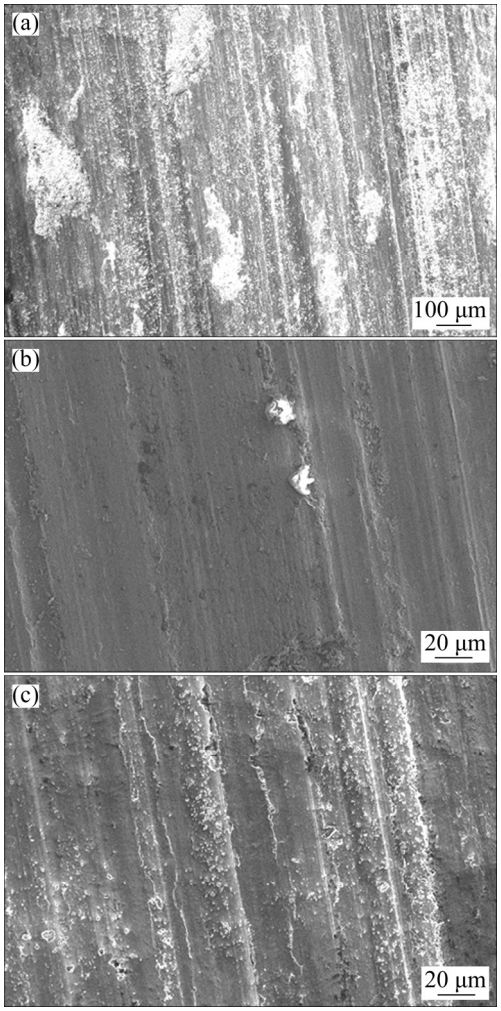

Fig. 11 Worn surface morphologies of HT alloy at 60 N load: (a) Overall image; (b) Adhesion region and presence of intact Si particle; (c) Presence of oxides

At 60 N load, the cumulative wear behavior of HT alloy exhibits similar trend (Fig. 9(a)) as is observed in AR alloy (Fig. 4(a)). After initial rapid wear, continuous resistance to further wear is seen from Fig. 9(a) at 60 N load (slope decreases at points *b* and *c* as shown in Fig. 9(a)). Accordingly, coefficient of friction plot in Fig. 9(b) exhibits decreasing trend with sliding distance and coefficient of friction remains almost steady between points *b* and *c*. The initial wear is attributed to abrasive (Fig. 11(a)) and adhesive wear (Fig. 11(b)). However, Si particles on the worn surface (Fig. 11(b)) provide resistance to abrasive wear, resulting in less total cumulative wear compared with AR alloy at 60 N load. Presence of adherent oxide and strain hardening effect under higher load is responsible for resistance to further wear.

3.2.2 Surface strain hardening

Microhardness values for α(Al) in AR and HT alloy are shown in Fig. 12. Microhardness values in all the specimens at all loads are found to be higher compared with the virgin specimens (without wear). However, there is a no particular trend with which microhardness

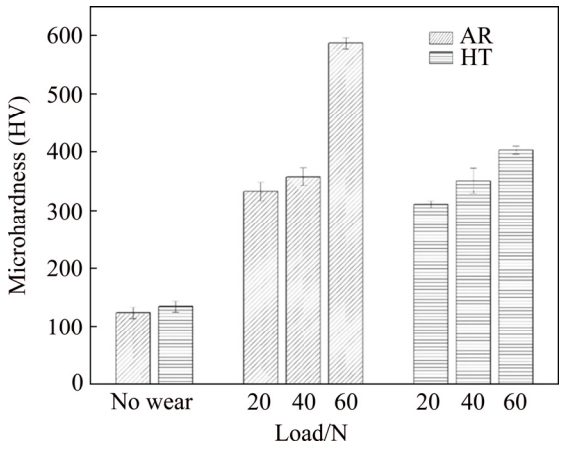

Fig. 12 Microhardness values of α(Al) for AR and HT alloys at different loads

values can be correlated to the applied loads for both AR and HT alloy. It is reported in the literature [19] that thermal softening also occurs during wear due to frictional heat generation apart from strain hardening. Moreover, delamination wear causes fresh surface to appear on the worn surface during wear process. This newly appeared surface will again experience strain hardening and thermal softening. Thus, microhardness values are dependent on the final state of the pin surface (i.e., after wear test). Therefore, it is not feasible to relate microhardness values of worn surface with loads. However, strain hardening of the worn surface is unambiguously established.

3.2.3 Overall wear rate

Wear rate plots for AR and HT alloy are shown in Fig. 13. It can be seen that wear rate increases with applied load for all specimens. This is in agreement with available literature. LIN et al [20] reported similar variation in wear rate with applied load for rheocast Al−17Si−2Cu−1Ni alloy. At any normal load, HT alloy exhibits lower wear rate as compared to AR alloy, indicating superior wear resistance property. This is due to the wear resistance offered by the nearly equiaxed/globular Si particles in HT alloy. The presence of such particles on the wear surface can be readily seen in Figs. 8(c), 10(b) and 11(b). Since the bonding between equiaxed/spherical particle and matrix is good due to minimization of surface area per unit volume in case of HT alloy, they are not removed easily during wear. On the other hand, due to high aspect ratio of Si particles (particularly eutectic Si particles having aspect ratio of 7±1.3), they maintain large contact area per unit volume and thus are easily removed during wear and evidences of such impression of particle removal are seen in Figs. 5(b), 6(b) and 7(b). In addition, the hardness of HT alloy is higher (Table 2) compared with AR alloy, which would result in less overall wear rate in HT alloy. From Fig. 13, it is also seen that the overall wear rate increases with a decreasing rate beyond 40 N load in both the alloys. This is attributed to the formation of adherent oxides due to frictional heat generation at higher load of 60 N. These oxides act as lubricant and thus lower the overall wear rate.

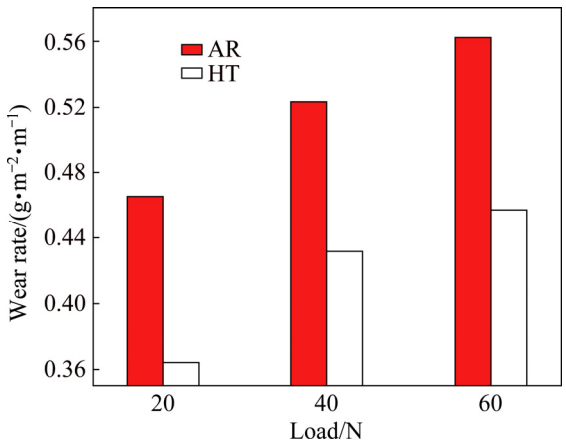

Fig. 13 Wear rates for AR and HT alloy at varying applied loads

4 Conclusions

1) AR alloy possesses microstructure consisting of primary Si particles and acicular/rod-like eutectic Si particles in a matrix of α(Al) grains. On isothermal heat treatment of this alloy, considerable microstructural modifications are observed. Accordingly, hardness value of HT alloy is found to be higher than that of AR alloy.

2) In general, the micro mechanism of wear during dry sliding wear test involves abrasion, adhesion (coupled with subsurface cracking) along with mild oxidation at 20 and 40 N loads. Whilst at higher load (60 N), adherent oxide formation is observed along with abrasive and adhesive wear. Thus, at higher load, the abrasive wear mechanism results in rapid wear loss at the beginning of the test. However, adherent oxides form on the worn surface due to frictional heating which provides continuous resistance to further wear. Moreover, significant strain hardening occurs on the worn surface at all loads.

3) The overall wear rate increases with load in all the specimens. However, the rate of increase decreases beyond 40 N load for both the alloys. This is attributed to the formation of adherent oxide layer and greater strain hardening effect at higher (60 N) load.

4) The overall wear rate for HT alloy is found to be significantly lower compared with as-cast (AR) alloy at all the applied loads, indicating remarkable improvement in wear resistance on isothermal heat treatment of AR alloy. Si particles (particularly eutectic), being acicular/rod-like in AR alloy, are removed easily during wear, the impressions of which are seen on worn surface. On the other hand, Si particles become spherical/equiaxed on isothermal heat treatment, which bonds strongly with the matrix. Thus, they remain intact during wear and provide resistance to abrasive wear. Moreover, the hardness increases on semisolid heat treatment, which further causes resistance to abrasive wear. Therefore, the combined effect of intact Si particles on the worn surface and higher hardness in isothermal heat-treated alloy result into superior wear resistance at all loads compared with as-cast alloy.

Acknowledgments

Authors acknowledge DST-SERB grant, vide Project No. YSS/2014/000172 dated 2015−08−17.

References

[1] VIJEESH V, PRABHU K N. Review of microstructure evolution in hypereutectic Al−Si alloys and its effect on wear properties [J]. Transactions of the Indian Institute of Metals, 2014, 67(1): 1−18.

[2] LASA L, RODRIGUEZ-IBABE J M. Effect of composition and processing route on the wear behaviour of Al−Si alloys [J]. Scripta Materialia, 2002, 46(6): 477−481.

[3] HU Zhao-hua, WU Guo-hua, XU Jia, MO Wen-fei, LI Yan-lei, LIU Wen-cai, ZHANG Liang, DING Wen-jiang, QUAN Jonathan, CHANG Yuan-wei. Dry wear behavior of rheo-casting Al−16Si−4Cu−0.5Mg alloy [J]. Transactions of Nonferrous Metals Society of China, 2016, 26(11): 2818−2829.

[4] CLARKE J, SARKAR A D. Wear characteristics of as-cast binary aluminium-silicon alloys [J]. Wear, 1979, 54: 7−16.

[5] ELMADAGLI M, ALPAS A T. Progression of wear in the mild wear regime of an Al−18.5%Si (A390) alloy [J]. Wear, 2006, 261: 367−381.

[6] JORSTAD J L. The hypereutectic aluminum−silicon alloy used to cast the Vega engine block [J]. Modern Casting, 1971, 60(4): 59−64.

[7] JORSTAD J L. The progress of 390 alloy: From inception until now [J]. AFS Transactions, 2009, 117: 241−249.

[8] ERGINER E. The strengthening of aluminum due to its cast microstructure modified by silicon [D]. Providence, USA: Brown University, 1969: 206.

[9] KIM Jewoosoo, JANG Gwang-Seon, KIM Mok-Soon, LEE Jeong-Keun. Microstructure and compressive deformation of hypereutectic Al−Si−Fe based P/M alloys fabricated by spark plasma sintering [J]. Transactions of Nonferrous Metals Society of China, 2014, 24(7): 2346−2351.

[10] FATHY N. Microstructural evolution of hyper-eutectic Al−18%Si alloy during semi-solid isothermal heat treatment [J]. International Journal of Research in Chemical, Metallurgical and Civil Engineering, 2014, 1(1): 5−9.

[11] ASTM E112–10. Standard test methods for determining average grain size [S]. West Conshohocken, PA: ASTM International, 2010.

[12] SHUKLA N, ROY H, SHOW B K. Tribological behaviour of a 0.33% ‘C’ dual phase steel with pre I/C ‘hardening and tempering’ treatment under abrasive wear condition [J]. Tribology Transactions, 2016, 59(4): 593−603.

[13] ASTM G99−05. Standard test method for wear testing with a pin-on-disk apparatus [S]. West Conshohocken, PA: ASTM International, 2010.

[14] KUMAR D, ROY H, SHOW B K. Triological behaviour of an aluminium matrix composite with Al_4SiC_4 reinforcement under dry sliding condition [J]. Tribology Transactions, 2015, 58: 518−526.

[15] DAS P, SHOW B K, RATHORE A, SAMANTA S. Wear behaviour of cooling slope rheocast A356 Al alloy [J]. Tribology Transactions, 2015, 58: 1054−1066.

[16] DEUIS R L, SUBRAMANIAN C, YELLUP J M. Dry sliding wear of aluminium composites—A review [J]. Composites Science and Technology, 1997, 57: 415−435.

[17] WANG S Q, WEI M X, ZHAO Y T. Effects of the tribo-oxide and matrix on dry sliding wear characteristics and mechanisms of a cast steel [J]. Wear, 2010, 269: 424−434.

[18] STOTT F H. The role of oxidation in the wear of metals [J]. Tribology International, 1998, 31: 61−71.

[19] LIM S C, ASHBY M F. Overview No. 55 wear-mechanism maps [J]. Acta Metallurgica, 1987, 35(1): 1−24.

[20] LIN Chong, WU Shu-sen, LÜ Shu-lin, ZENG Jin-biao, AN Ping. Dry sliding wear behavior of rheocast hypereutectic Al−Si alloys with different Fe contents [J]. Transactions of Nonferrous Metals Society of China, 2016, 26(3): 665−675.

热处理工艺提高 Al−17Si−5Cu 合金的干滑动耐磨性

Biplab HAZRA, Pankaj BARANWAL, Supriya BERA, Bijay Kumar SHOW

Department of Metallurgical and Materials Engineering,
National Institute of Technology Durgapur, West Bengal, 713209, India

摘　要：通过等温热处理调整铸态 Al−17Si−5Cu (AR)合金中 Si (尤其是共晶 Si) 颗粒的形貌以提高合金的耐磨性能。通过销−盘式摩擦机对比研究热处理后的合金 (HT 合金) 和 AR 合金的磨损行为，并采用扫描电镜观察磨损表面。结果表明，HT 合金的显微组织发生显著变化，相应地，HT 合金较 AR 合金的硬度值增大。与 AR 合金相比，HF 合金在所有载荷下总磨损率明显降低，耐磨性能明显改善。热处理后，共晶 Si 颗粒由针/棒状变为球形/等轴状(长径比接近 1)，与基体形成良好结合，在磨损过程中保持完整且更加坚硬，为材料提供良好的耐磨性。另外，HT 合金硬度的增加进一步提高合金的耐磨性。因此，完整且较硬的 Si 颗粒对磨损表面的作用以及材料整体硬度的提高导致 HT 合金在所有载荷下的磨损行为均优于 AR 合金。

关键词：热处理；磨粒磨损；过共晶铝硅合金

(Edited by Bing YANG)